Electronic Supporting Information (ESI)

Electrochemical and thermodynamic processes of metal nanoclusters enabled biorealistic synapses and leaky-integrate-and-fire neurons

*Jingxian Li[ab], Yuchao Yang[*a], Minghui Yin[a], Xinhao Sun[a], Lidong Li[*b], and Ru Huang[*a]*

a. Key Laboratory of Microelectronic Devices and Circuits (MOE), Institute of Microelectronics, Peking University, Beijing 100871, China. E-mail: yuchaoyang@pku.edu.cn, ruhuang@pku.edu.cn

b. State Key Lab for Advanced Metals and Materials, School of Materials Science and Engineering, University of Science and Technology Beijing, Beijing 100083, China. E-mail: lidong@mater.ustb.edu.cn

XPS characterization of Ta_2O_5 film

We have measured the Ta 4*f* XPS spectrum of as-deposited Ta_2O_5 film (Figure S1), which can be deconvolved into a dominant Ta 4*f* doublet with Ta $4f_{7/2}$ and $4f_{5/2}$ peaks located at 26.35 and 28.25 eV, respectively. These peaks are characteristics of Ta^{5+} state (Ref. S1). Since the existence of oxygen vacancies in Ta_2O_5 should result in sub-oxidic state of Ta (Ref. S2), the almost absence of such sub-oxidic Ta states in Figure S1 is consistent with the RF sputtered Ta_2O_5 films with roughly maintained stoichiometry.

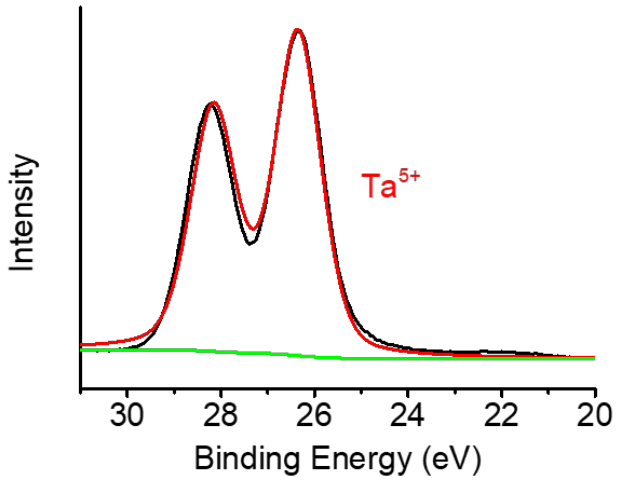

Figure S1. Ta 4*f* XPS spectra obtained from as-deposited Ta_2O_5 film. Red lines correspond to Ta 4*f* doublets from the fully oxidic state.

Electrical characterization

Figure S2 shows the current response of a Pd/Ag-NCs/Ta_2O_5/Pd device when a pulse train containing 5 identical voltage pulses (0.6 V, 100 ms) was applied, where similar short-term and long-term plasticity with that in Ta/Ag-NCs/Ta_2O_5/Pt/Ti devices can be observed. Since a Ta electrode is missing in the Pd/Ag-NCs/Ta_2O_5/Pd structure, it demonstrates that the top electrode material does not play an important role in the resistive switching. This is consistent with that physical picture where the resistive switching in the devices is dominated by the migration and redistribution of Ag nanoclusters instead of oxygen vacancies, as supported by detailed high resolution TEM and EDS characterization in Figure 2.

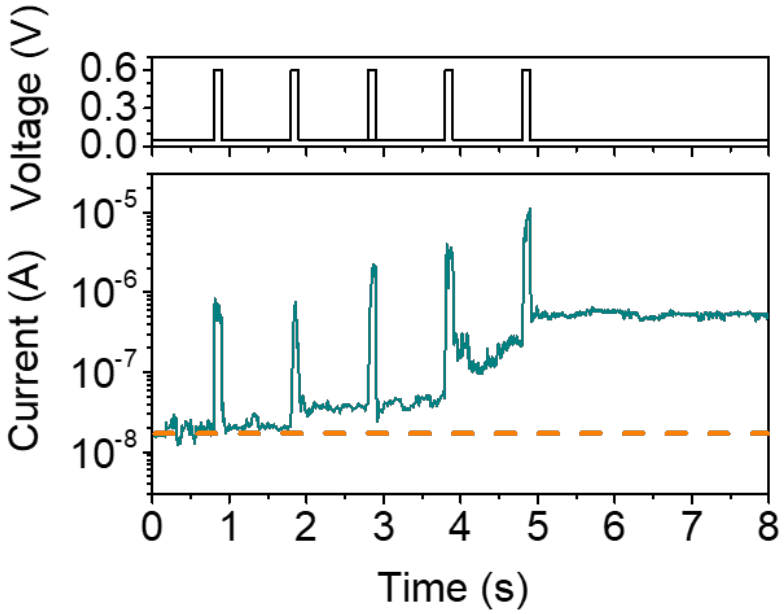

Figure S2. Synaptic plasticity in Pd/Ag-NCs/Ta_2O_5/Pd devices. A train of five voltage pulses (0.6 V, 100 ms) were applied, indicating a transition from STP to LTP.

Figure S3 shows the *I-V* characteristics of the Ta/Ag-NCs/Ta_2O_5/Pt/Ti device. The sharp switching characteristics and large on/off ratio are in agreement with resistive switching as a result of metal filament formation, instead of valence change mechanism. Combined with the detailed high resolution TEM and EDS characterization in Figure 2, the resistive switching in the present devices should be purely modulated by the Ag-NCs evolution instead of oxygen vacancies. After the positive sweep is finished and the applied voltage returns to zero, the device automatically switches back to off state, as shown in the 2nd sweep toward negative direction. Such volatile nature is in agreement with the short-term plasticity of the device, where a weak Ag filament has been formed in previous sweeping but spontaneously breaks into discrete nanoclusters, as depicted in Figure 2e-h.

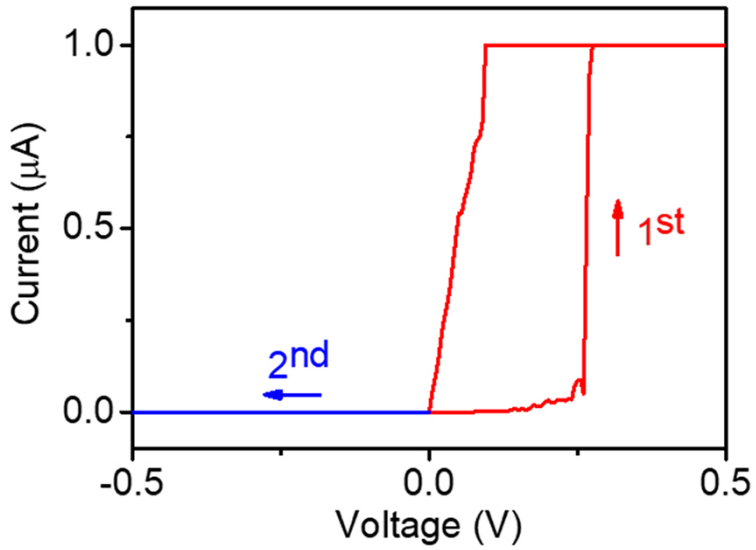

Figure S3. *I-V* characteristics of the Ta/Ag-NCs/Ta_2O_5/Pt/Ti device.

The log-scale *I-V* sweep of the device is shown in Figure S4. From the bipolar cycles with different I_{cc}, a clear understanding about the filament growth and rupture can be obtained. When an I_{cc} of 1 μA was used, the device exhibited volatile switching and returned to high resistance state when the voltage was reduced to zero, as indicated by the absence of hysteresis in the negative voltage direction. This can be attributed to the fact that the filament has spontaneously broken into discrete nanoclusters, as depicted in Figure 2h, in order to minimize the surface energy of the Ag filament and reach thermodynamic equilibrium after removing the electrical signals. If the I_{cc} was increased to 100 μA, nonvolatile switching happened in the positive voltage direction and then could be reset in the negative cycle. Such bipolar nonvolatile switching behavior implies high Ag concentration in the dielectric. The volatile to nonvolatile transition achieved by controlling the current compliance value is in agreement with the STP to LTP transition by tuning pulse parameters (Figure 1), which can all be explained by the Ag dynamics in the devices (Figure 2).

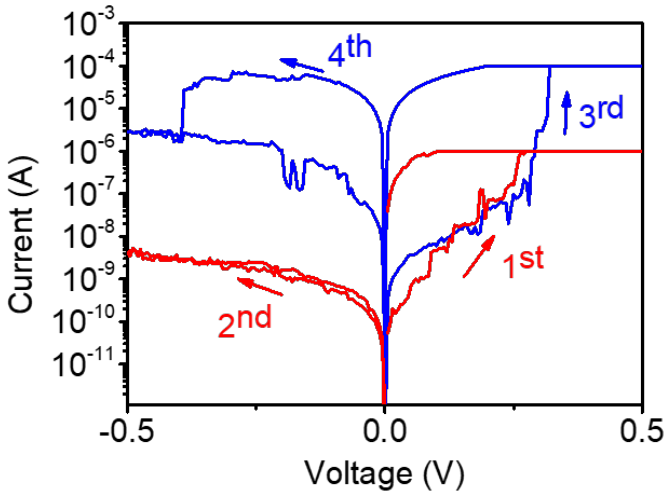

Figure S4. Log-scale *I-V* characteristics of the device with different compliance currents. a) Unipolar volatile switching characteristics of the device measured under 1 μA compliance current. b) Bipolar nonvolatile switching characteristics of the device measured under 100 μA compliance current.

Electric tunneling in LTP state

We have measured the remnant thickness of the insulating layer after Ag accumulations at both cathode and anode interfaces, and found the effective thickness has been reduced to ~4 nm (Figure S5), compared with the 7.7 nm in the pristine state where the Ag clusters only reside at the top interface. It should be noted that only a thin lamella of the sample was observed during the cross sectional TEM due to the sample preparation procedure. The region observed may not be the most critical switching area, and hence the remnant thickness of the insulating layer should be equal with or even smaller than 4 nm, making electric tunneling possible. In order to further confirm the tunneling mechanism, we have performed temperature dependent electrical measurements on in devices showing LTP, as shown in Figure S6. One can clearly see a weak dependence of the device conductance on temperature, further demonstrating the electric tunneling between the Ag clusters.

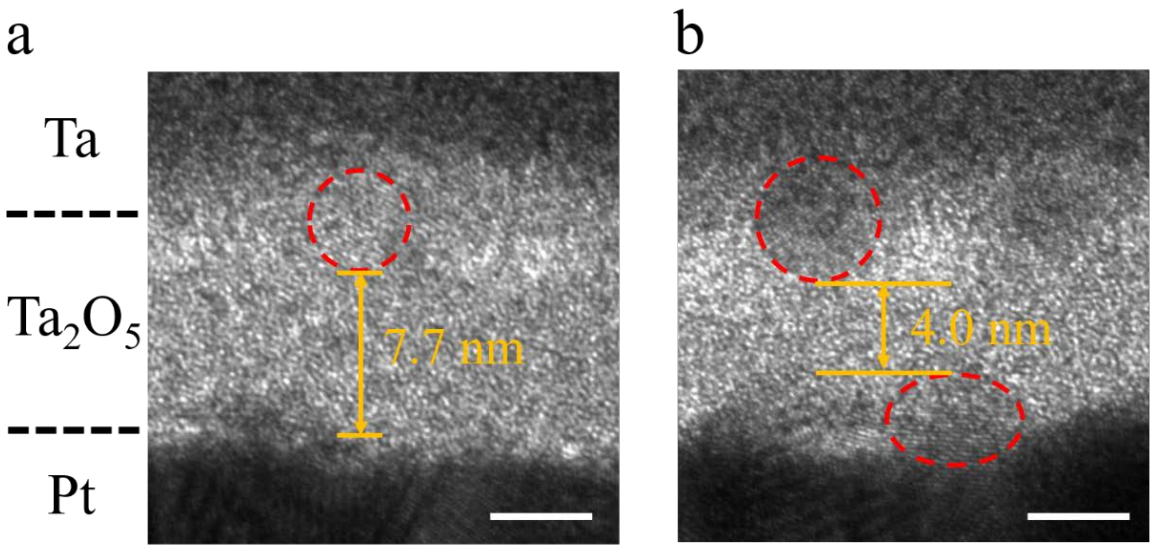

Figure S5. High resolution TEM of a) a pristine device and b) a device showing long-term plasticity.

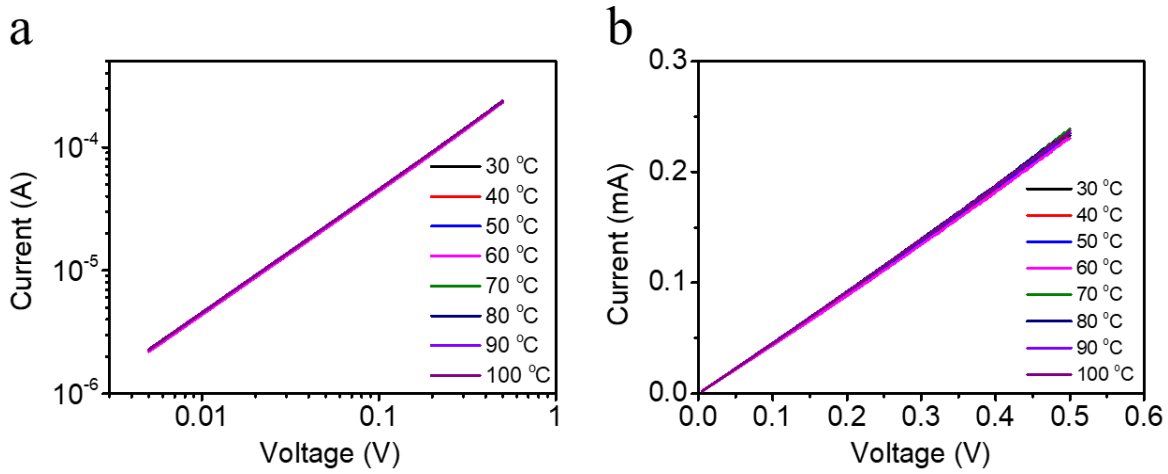

Figure S6. *I-V* curves of the LRS in a) linear scale and b) log scale measured at different temperatures ranging from 30 to 100 °C.

As a control experiment, Figure S8 shows the cross sectional TEM images and corresponding EDS mapping at Ag L edge from Ta/Pd-NCs/Ta_2O_5/Pt/Ti devices under similar programming conditions, where the Ag nanoclusters were replaced by Pd nanoclusters. Corresponding TEM and EDS results showed that the Pd nanoclusters were immobile under such field intensity and still concentrated at the top electrode interface (Figure S7). The different behaviors of Ag-NCs and Pd-NCs highlights the role of mobile Ag-NCs in enabling the STP and LTP behaviors.

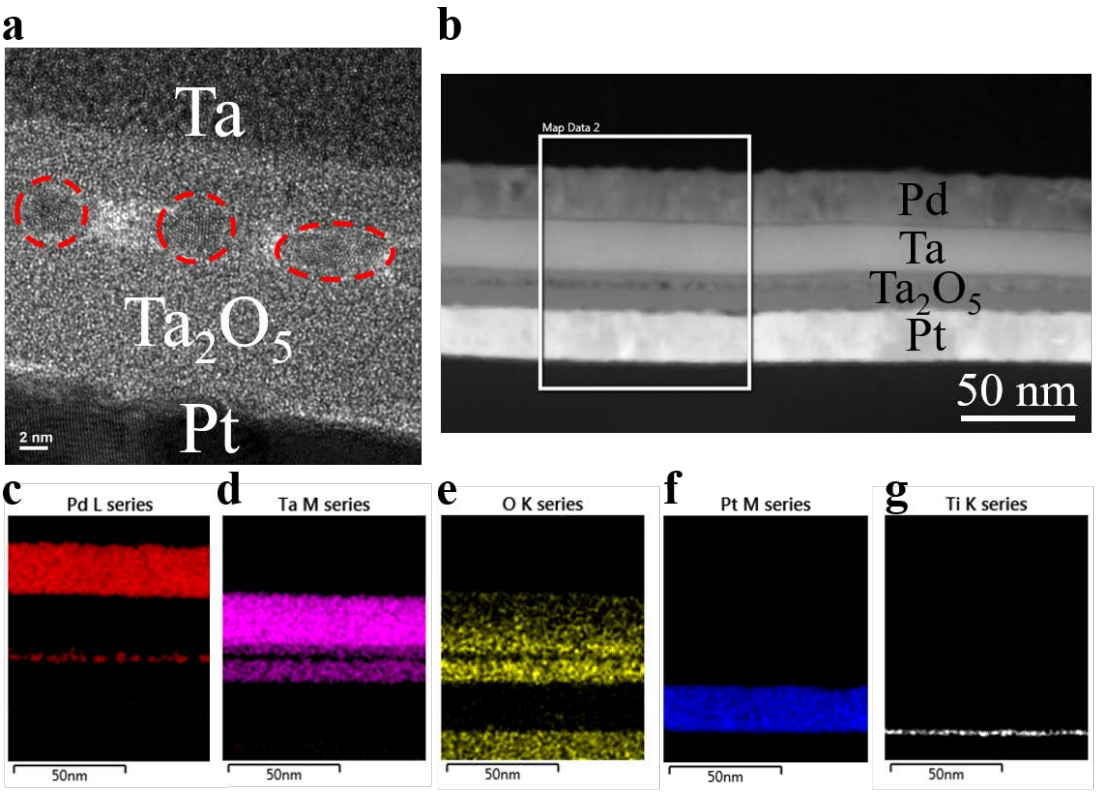

Figure S7. Microstructural and compositional analyses of the Ta/Pd-NCs/Ta_2O_5/Pt/Ti devices after resistive switching. a) High resolution TEM image of a Ta/Pd-NCs/Ta_2O_5/Pt/Ti device after set process. The red dotted ovals show the presence of Pd nanoclusters near the top electrode. b) cross-sectional scanning transmission electron microscopy image of the device. c-g) EDS mapping of Pd L, Ta M, O K, Pt M, Ti K edges inside the white dotted box region in (b).

The relatively wide pulse width was selected due to a compromise between the current measurement sensitivity and sampling interval limit of the test equipment. The measurement setup in this work includes an Agilent B1500A semiconductor parameter analyzer and an Agilent B1530A waveform generator/fast measurement unit. The high resistance state of our devices can reach pA level, as can be seen in log-scale pulse measurement results (Figure 3a-g). While Agilent B1500A semiconductor parameter analyzer possesses sufficiently high current measurement sensitivity, the minimum sampling interval is 2 ms, therefore we have to set pulses with a large width (100 ms) in order to include enough data points and show the

waveform within a single pulse duration clearly. In contrast, Agilent B1530A waveform generator/fast measurement unit can have much faster sampling with a minimum sampling interval of 5 ns, however the current has to be higher than 1 μA, which cannot probe the device characteristics clearly in higher resistance state. As a result, a pulse width of 100 ms was adopted in the present study, and it doesn't reflect the operation speed of the device. In order to verify this, we have started the measurements from a more conductive state so that the measurements can be performed using B1530A with better temporal resolution. One can see that EPSC and STP–LTP transition can once again be achieved by application of pulses with a reduced width of 10 μs, as shown in Figure S8.

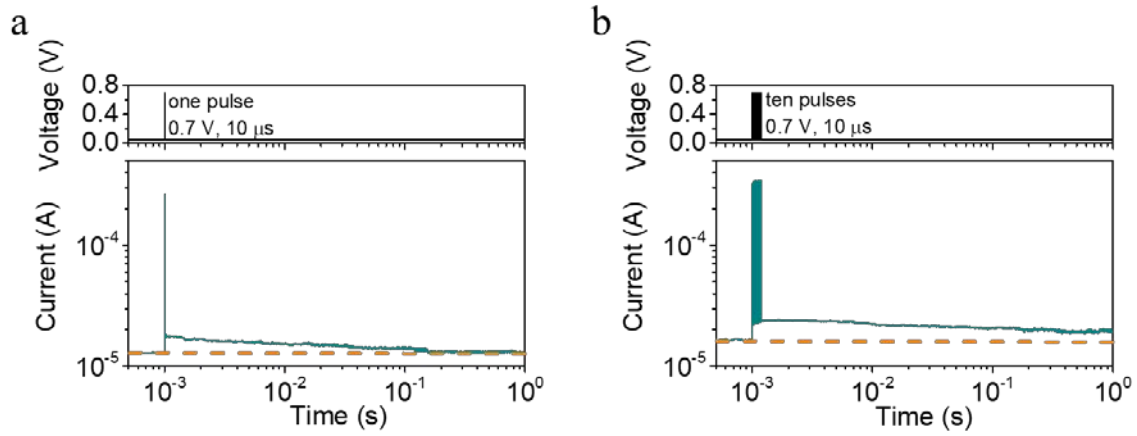

Figure S8. EPSC and STP–LTP transition. a) Current response to a voltage pulse (0.7 V, 10 μs), indicating EPSC characteristic. b) Current response to a train of ten voltage pulses (0.7 V, 10 μs) with 10 μs pulse interval, indicating a transition from STP to LTP.

Artificial neuron characteristics

In order to demonstrate the leaky property clearly, we have tested two consecutive cycles of neuron activity, and a longer rest period of 13.5 ms after firing can fully return the artificial neuron back to its resting state, as can be seen in Figure S9, even without a reset operation. This might be due to the fact that the firing threshold of 3 μA still corresponds to a volatile resistance state.

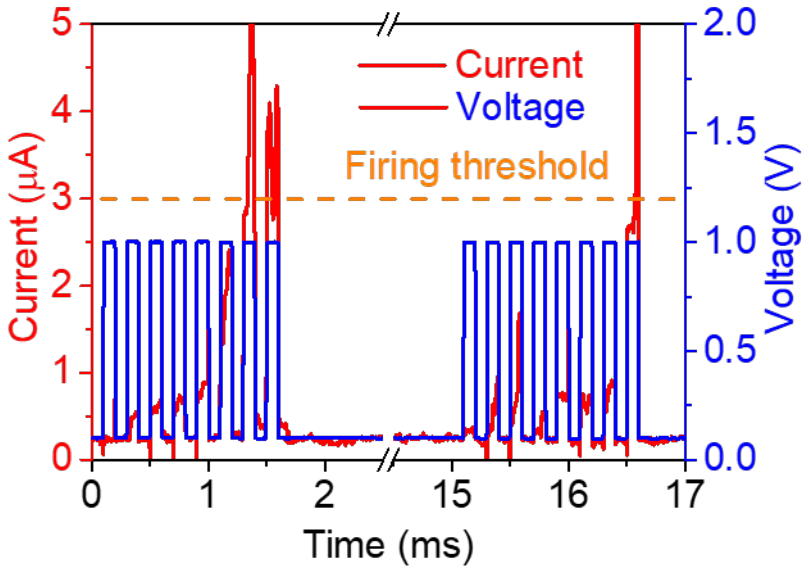

Figure S9. Two consecutive cycles of neuron activity with a rest period of 13.5 ms.

Method of training array with the classical conditioning

As an example of potential applications in neuromorphic systems, the classical conditioning could be used to learn and detect temporal correlations in event-based data streams based on unsupervised learning. Specially, one of the event-based data stream can be converted to conditional stimulus (CS) and serve as input to one of the rows, while the other event-based data stream can be converted to unconditional stimulus (US) (however with a negative value since it is applied to the bottom electrode) and serve as input to one of the columns, as depicted in Figure S10. Based on the asynchronous classical conditioning in our devices shown in Figure 4e-h, temporal correlation between these two event-based data streams could be learnt and detected physically, manifesting as an increase of the synaptic weight at the corresponding crosspoint. Such detection of temporal correction could be useful for understanding the internal correlations between unlabeled data.

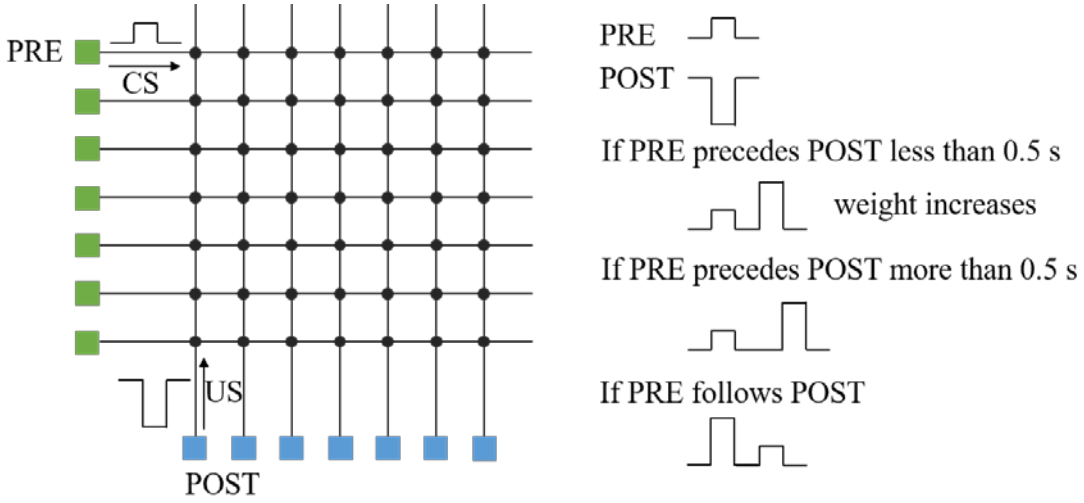

Figure S10. Crossbar circular and pulses for classical condition. Only when the PRE precedes POST less than 0.5 s, the memristor's conductance is increased.

References

S1. E. Atanassova, T. Dimitrova, J. Koprinarova, *Appl. Surf. Sci.* **1995**, 84, 193.

S2. M. J. Lee, C. B. Lee, D. Lee, S. R. Lee, M. Chang, J. H. Hur, Y. B. Kim, C. J. Kim, D. H. Seo, S. Seo, U. I. Chung, I. K. Yoo, K. Kim, *Nat. Mater.* **2011**, 10, 625.

S3. T. Hasegawa, T. Ohno, K. Terabe, T. Tsuruoka, T. Nakayama, J. K. Gimzewski, M. Aono, *Adv. Mater.* **2010**, 22, 1831.